Acta Pharmaceutica Sinica B 2022;12(1):394–405

Chinese Pharmaceutical Association
Institute of Materia Medica, Chinese Academy of Medical Sciences

Acta Pharmaceutica Sinica B

www.elsevier.com/locate/apsb
www.sciencedirect.com

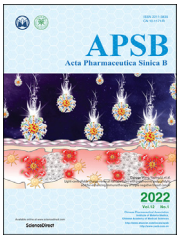

ORIGINAL ARTICLE

Accurate construction of cell membrane biomimetic graphene nanodecoys *via* purposeful surface engineering to improve screening efficiency of active components of traditional Chinese medicine

Qi Hu[a,b], Lanlan Jia[a,b], Xiaolin Zhang[a,b], Aihong Zhu[a,b], Sicen Wang[a,b], Xiaoyu Xie[a,b,*]

[a]*School of Pharmacy, Health Science Center, Xi'an Jiaotong University, Xi'an 710061, China*
[b]*Shaanxi Engineering Research Center of Cardiovascular Drugs Screening & Analysis, Xi'an 710061, China*

Received 6 March 2021; received in revised form 9 April 2021; accepted 12 April 2021

KEY WORDS

Cell membrane;
Biomimetic nanoengineering;
Purposeful surface engineering;
Graphene oxide;
Dispersity;
Active components screening;
Traditional Chinese medicine;
PEGylation

Abstract Biomimetic nanoengineering presents great potential in biomedical research by integrating cell membrane (CM) with functional nanoparticles. However, preparation of CM biomimetic nanomaterials for custom applications that can avoid the aggregation of nanocarriers while maintaining the biological activity of CM remains a challenge. Herein, a high-performance CM biomimetic graphene nanodecoy was fabricated *via* purposeful surface engineering, where polyethylene glycol (PEG) was used to modifying magnetic graphene oxide (MGO) to improve its stability in physiological solution, so as to improve the screening efficiency to active components of traditional Chinese medicine (TCM). With this strategy, the constructed PEGylated MGO (PMGO) could keep stable at least 10 days, thus improving the CM coating efficiency. Meanwhile, by taking advantage of the inherent ability of HeLa cell membrane (HM) to interact with specific ligands, HM-camouflaged PMGO showed satisfied adsorption capacity (116.2 mg/g) and selectivity. Finally, three potential active components, byakangelicol, imperatorin, and isoimperatorin, were screened from *Angelica dahurica*, whose potential antiproliferative activity were further validated by pharmacological studies. These results demonstrated that the purposeful surface

*Corresponding author. Tel./fax: +86 29 82656788.
E-mail address: xiexiaoyu@xjtu.edu.cn (Xiaoyu Xie).

Peer review under responsibility of Chinese Pharmaceutical Association and Institute of Materia Medica, Chinese Academy of Medical Sciences.

https://doi.org/10.1016/j.apsb.2021.05.021

engineering is a promising strategy for the design of efficient CM biomimetic nanomaterials, which will promote the development of active components screening in TCM.

1. Introduction

Cell membrane (CM)-camouflaged nanomaterials represent an emerging and interesting biomimetic platform, which become increasingly prevalent in biomedical research[1−4]. To date, nanomaterials with unique properties such as carbon nanotube[5] and magnetic particles[6] have been employed to develop CM-camouflaged nanomaterials. By transferring the membrane directly onto the surface of the nanomaterials, the complexity of the membrane, including its proteins, carbohydrates, and lipids, can be completely preserved, enabling the synthetic CM-camouflaged nanomaterials to possess many of the characteristics exhibited by the source cell[7−10]. In particular, by taking advantage of the inherent ability of CM to interact with specific ligands, CM-camouflaged nanomaterials have enhanced targeting capability, showing an attractive prospect in the affinity recognition field[11−13]. Promising results have also recently emerged in potential active components screening in traditional Chinese medicine (TCM)[14−16].

From nanomaterials synthesis point of view, the typical top-down pathway is currently in a leading position for CM camouflage to nanocarriers, because it excludes tedious chemical synthesis and causes negligible damage on the composition of CM and the function of nanocarriers[17,18]. However, the interfacial interactions between CM and nanocarriers affect whether the CM can be camouflaged onto the nanocarriers effectively[19,20]. For instance, nanocarriers have a strong tendency to accumulate in salt-containing or physiological media owing to the existence of static charges, which greatly reduce the binding area, resulting in a low membrane-coating rate[21]. Hence, a critical challenge to the top-down pathway is how to avoid the aggregation of the nanocarriers before the membrane camouflage while maintaining the bioactivity of the CM.

Given the importance of nanomaterials biointerfacing, the purposeful surface engineering is a critical part of the top-down pathway, which can be employed to settle the issues described above[22]. With a high surface area, good biocompatibility, and sufficient surface groups, graphene oxide (GO) can be used as a unique double-sided and easily accessible nanocarrier for efficient loading of CM[23−26]. The intrinsic chemical composition and lateral size of GO have a certain influence on its dispersity, which leads to aggregation in the process of CM coating. It is worth noting that the well-functionalized GO modified by a variety of biocompatible polymers showed a significant improvement in dispersity[27−29]. Inspired by this, we expected that the biocompatible polymer modification could greatly increase the interfacial interaction between the CM and GO, resulting in a high membrane coating efficiency. Among various biocompatible polymers, polyethylene glycol (PEG) is a very useful modification material due to its remarkable hydrophilicity, low cytotoxicity, and biocompatibility[30−35]. Hence, it was expected that the surface modification of GO using PEG plays an important role in improving the CM coating efficiency and enhancing the selectivity of active components screening from TCM.

Herein, the novel CM biomimetic graphene nanodecoys with improved screening efficiency were prepared *via* the purposeful surface engineering. During this procedure, the PEGylated magnetic GO (PMGO) was synthesized, and then coated with CM from HeLa cells through an optimized top-down approach. Among all the CM sources, the pathological tissues are the most ideal materials for screening active components from TCM due to the maximum imitation of *in vivo* drug−receptor interactions[36]. Hence, HeLa cell membrane (HM) was incorporated as the coating of PMGO to provide nanodecoys (HPMGO) in view of the above merits. In addition, magnetic nanoparticles were introduced as the magnetic assistance to help efficiently separate the nanodecoys. The morphological characterization and adsorption properties of the resultant HPMGO were systematically evaluated. We found that the conjugation of PEG effectively enhanced the dispersity of magnetic GO (MGO) in physiological solutions, and the HM coating efficiency was further enhanced. Furthermore, the HPMGO demonstrated better efficiency for screening active components from TCM owing to the improved coating amounts of HM. Ultimately, our results indicated the broad applicability of the purposeful surface engineering for CM-camouflaged nanomaterials, which will promote the rapid development of this emerging biomimetic nanotechnology and open up a new path for the study on active components of TCM.

2. Materials and methods

2.1. Materials and regents

GO was purchased from XFNANO material Tech. Co., Ltd. (Nanjing, China). Iron (III) chloride hexahydrate ($FeCl_3 \cdot 6H_2O$), ethylene glycol (EG), and sodium acetate (NaAc) were provided by Guanghua Tech. Co., Ltd. (Guangzhou, China). Six-armed polyethyleneglycol with six amino end groups (6-armed PEG−NH_2) was obtained from Ponsure Biotech. Inc. (Shanghai, China). DMEM, trypsin, fetal bovine serum (FBS), and *N*-(3-(dimethylamino)propyl)-*N*′-ethylcarbodiimide hydrochloride (EDC·HCl) were offered by Sigma−Aldrich LLC. (St. Louis, MO, USA). Verapamil, tamsulosin, and valsartan were obtained from Ange Pharmaceutical Co., Ltd. (Nanjing, China). Vinorelbine ditartrate, fluorescein Isothiocyanate (FITC), coomassie brilliant blue R250, PAGE gel quick preparation kit, hoechst 33,258 stain solution, and annexin V-FITC/PI apoptosis assays kit were offered by Yeasen Bio. Tech. Co., Ltd. (Shanghai, China). Byakangelicol, imperatorin, and isoimperatorin were obtained from Herbest Bio. Tech. Co., Ltd. (Baoji, China).

2.2. Preparation of HPMGO

At first, MGO was synthesized *via* a previously described solvothermal approach[26]. In brief, GO (85 mg) was suspended in EG (6 mL) and ultrasonicated for 1 h $FeCl_3 \cdot 6H_2O$ (320 mg) was added, followed by ultrasonic treatment for 30 min, and then sodium acetate (300 mg) was added and stirring for 30 min at 50 °C. The mixture was then heated to 200 °C in a stainless-steel autoclave for 6 h. The obtained MGO were collected by external magnetic field, and then purified by washing sequentially with methanol and water each three times.

To enhance the dispersity of MGO, PEG was conjugated according to a previously reported approach with a minor modification[32]. For the PEGylation of MGO, 6-armed PEG−NH_2 was employed as the PEG coupling reagent, while EDC·HCl was used as the carboxyl activator to enable the formation of amide bond during the chemical conjugation. MGO supernatant was pretreated with NaOH followed by bath-sonicated with 10 mg/mL 6-armed PEG−NH_2 for 5 min. EDC was then added to reach 5 mmol/L and the solution was bath sonicated for another 30 min, followed by adding enough EDC to reach 20 mmol/L and stirring for 12 h. Dialysis (MW_{cutoff} = 14 kDa) was used to purify the initial product for 3 days, and the unbound 6-armed PEG−NH_2 was removed to finally obtain PMGO.

HeLa cells were cultured in a humidified atmosphere (5% CO_2) at 37 °C with DMEM medium containing FBS (10%) and penicillin/streptomycin (1%). HM was prepared following a previously published approach[15]. The resulting pellets of HM were lyophilized and stored at −80 °C. The protein amounts were determined by the bicinchoninic acid (BCA) protein assay kit (Yeasen Bio. Tech. Co., Ltd., Shanghai, China). The lyophilized membrane materials were rehydrated in PBS (pH = 7.4) prior to use. Then, the above PMGO was added into the HM under vortexing, followed by the ultrasonication at 4 °C for 10 min. Afterwards, the resulting products were further collected by magnetic field and washed to remove unbound HM.

2.3. Characterization of HPMGO

The surface morphologies of prepared materials were studied using JEOL JCM-5700 scanning electron microscopy (SEM; Welwyn Garden City, UK) and JEOL JEM-2100Plus transmission electronic microscopy (TEM; Tokyo, Japan). The chemical conjugation of PEG to MGO was confirmed by Fourier Transform Infrared Spectroscopy (FTIR; AVATAR-360 FTIR spectrophotometer, Madison, Wisconsin, USA). The element composition of MGO and PMGO was recorded on X-ray photoelectron spectroscopy (XPS; K-Alpha, Thermo Fisher, Waltham, MA, USA). Thermogravimetric analysis (TGA) was conducted on Discovery TGA 55 thermal analysis system (TA, New Castle, PA, USA) in N_2 with a heating rate of 10 °C/min. Surface charge of GO, PMGO, HM, and HPMGO in PBS buffer (pH 7.4) were confirmed by zeta potential measurements using dynamic light scattering (Malvern Zetasizer Nano S90, Malvern, UK). The magnetic property was assessed by Lake Shore 7307 vibrating sample magnetometer (VSM; Columbus, OH, USA).

2.4. Protein analysis and fluorescence characterization

The protein components of prepared materials were analyzed by using sodium dodecyl sulfate-polyacrylamide gel electrophoresis (SDS-PAGE). The HeLa cell, HM, and HPMGO were prepared in SDS sample buffer, and then various samples were loaded into each well of an 8% SDS gel. The resulting polyacrylamide gel was stained in Coomassie Blue and destained overnight for visualization. Before fusing HM and PMGO, HM was labelled with CM red fluorescent probe DiI (1,1′-dioctadecyl-3,3,3′,3′-tetramethylindocarbocyanine perchlorate, Beyotime Biotechnology Co., Ltd., Shanghai, China). Briefly, HM was mixed with DiI for 20 min. Excessive DiI was removed from HM by centrifugation and washed with PBS. Then DiI-labelled HM was further coated onto PMGO as described above. Meanwhile, PMGO was labelled by the same procedure as HPMGO in the absence of HM. Finally, the labelled materials were imaged using TCS SP8 STED 3X confocal laser scanning microscope (CLSM; Leica, Solms, Germany).

2.5. Stability study

The stability of PMGO dispersion was studied in different media including deionized water, normal saline, PBS buffer, and DMEM medium. During the given time intervals, the dispersity of PMGO in the tubes were photographed to intuitively reflect the changes over a period of time. MGO without PEG served as control.

2.6. In vitro targeting toward ligands

Adsorption selectivity experiment was used to investigate the ligands targeting ability of HPMGO. In brief, vinorelbine ditartrate (selective HeLa cell inhibitor) was employed as the positive drug, while verapamil (calcium channel blocker), tamsulosin (selective α1 adrenergic receptor blocker), and valsartan (angiotensin receptor blocker) were used as the negative control applied to the adsorption selectivity experiments. Samples of 10 mg HPMGO and non-HM-coated PMGO (NPMGO) were placed in centrifuge tubes, followed by the addition of 1 mL above ligands (100 μg/mL), respectively. These samples were ultrasonic dispersed and oscillated at 4 °C for 10 min in a constant temperature oscillator. After adsorption, the samples were separated and washed, and the concentration of all the supernatant was detected. The binding amounts equation as shown in Eq. (1):

$$Q = \frac{(C_0 - C_e) \times V}{m} \quad (1)$$

where C_0 (μg/mL) is the initial concentration of ligands, and C_e (μg/mL) is the residual concentration of ligands. V (mL) refers to the volume of ligands, and m (mg) refers to the amount of the adsorbent.

2.7. Potential active components screening from TCM

HPMGO was used as adsorbent to screen potential active components from TCM following an evaluation of targeted identification and ligand enrichment capabilities. The *Angelica dahurica* (1.0 g) was ground into fine powder and extracted with 20 mL ether for 1 h under oscillate. The filtrate was evaporated and dissolved in ethyl acetate. 5.0 mg HPMGO was dispersed in 1.0 mL crude extract to capture the potential bioactive ingredients binding to the receptor. The washing solvent was PBS-acetonitrile (9:1, *v*/*v*) and the elution solvent was PBS-acetonitrile (7:3, *v*/*v*). Under these conditions, we collected the elution solutions and identified the potential bioactive ingredients by HPLC−Q-TOF-MS/MS (Shimadzu Corporation, Kyoto, Japan).

2.8. Antiproliferative assay

The *in vitro* antiproliferative assay was measured by the CCK-8 assay (Cell Counting Kit-8, Beyotime Biotechnology Co., Ltd., Shanghai, China). First, HeLa cells were seeded into 96-well plates in 200 mL medium and subsequently cultured for 24 h. Then different concentrations of above bioactive ingredients were added to the wells, respectively, and further incubated for 24 h. In the end, 100 μL medium containing 10 μL CCK-8 was added, and incubated for another 1 h. Finally, the cell viability was measured using a microplate reader at a wavelength of 450 nm.

2.9. Apoptosis by hoechst 33,258 staining assay

Since the screened active components indicated significant cytotoxic potential on HeLa cells, the apoptotic effect was further evaluated to understand the cytological changes. HeLa cells (2×10^5) were seeded on 6-well plates and treated with the captured potential bioactive ingredients at the different concentrations for 48 h, respectively. After treatment, the cells were washed twice with PBS and stained with hoechst 33,258 solution for 20 min. The stained cells were further washed twice with PBS and then observed under a fluorescence microscope excited at 350 nm and emitted at 460 nm.

2.10. Cell apoptosis analysis

Apoptosis of HeLa cells was further evaluated with annexin V-FITC/PI apoptosis detection kit. For that, HeLa cells (2×10^5) were seeded on 6-well plates and incubated for 12 h. The cells were treated with the captured potential bioactive ingredients at different concentrations for 48 h, respectively. The cells were collected and washed twice with prechilled PBS, and further resuspended in 100 μL 1 × binding buffer. Next, 5 μL annexin V-FITC and 10 μL PI staining solution were added. After incubation at room temperature in dark for 10 min, 1 × binding buffer (400 μL) was added. The cells apoptosis was analyzed by a flow cytometer (ACEA biosciences, San Diego, CA, USA).

2.11. Statistical method

All data were taken from three independent experiments and presented as mean ± SD. Statistical analysis was performed using GraphPad Prism 5.0. Differences were considered significant at $^{*}P < 0.05$, $^{**}P < 0.01$, and $^{***}P < 0.001$.

3. Results and discussion

3.1. Preparation and protein analysis of HPMGO

The primary task of this work is to fabricate the well-functionalized MGO with excellent dispersity, which is critical for the following coating by HM to provide HPMGO with enhanced efficiency. As we know, nanomaterials were prone to aggregation due to the high surface energy and large specific surface area[37]. Chemical conjugation of various biocompatible polymers on the nanomaterials is the most commonly used method to improve the dispersity in aqueous medium[27]. Hence, to address above issue, we attempted to prepare a functionalized MGO with excellent dispersity by PEGylation.

Schematic representation of the preparation, application, and advancement of HPMGO were shown in Fig. 1. The design and preparation process were illustrated in Fig. 1A. At first, to construct HPMGO, PEG-modified MGO was synthesized. The resultant PMGO dispersed well in water. HM were prepared by emptying the intracellular contents through combining hypotonic lys, mechanical fragmentation, and gradient centrifugation. After that, PMGO were surface coated with the resulting HM by mixing the PMGO and HM. Fig. 1B and C exhibited the drug leads capture application and the dispersity improvement of HPMGO, respectively.

In order to obtain versatile HPMGO with high performance, the preparation process (Fig. 2A) was optimized. The amount of coated HM in PMGO was studied. For these study, FITC (488/525 nm) as a fluorescent probe was used to quantify attachment of HM. FITC was mixed with HM in PBS to form labeled HM (HM/FITC). Fig. 2B show emission spectra of HPMGO prepared by HM/FITC and MGO at different ratios. It was found that the fluorescence intensity enhanced significantly with the increase of HM concentration, and did not change until the ratio increased to 1:4, indicating that 1:4 was the optimum preparation condition. The coated HM amounts on PMGO were quantified by a BCA protein assay kit. The coating amount equation as shown in Eq. (2):

$$Q = \frac{(m_0 - m_e)}{m} \tag{2}$$

where Q (mg/g) represents the coating amount of HM. m_0 (mg) and m_e (mg) are the initial and equilibrium amounts of the HM, respectively. And m (mg) refers to the amount of PMGO. The result showed that the coating amount was 794.3 mg/g.

3.2. Dispersity of PMGO in different medium

As mentioned above, the dispersity of the prepared PMGO in the aqueous medium was crucial for the membrane coating. Thus, in order to illustrate the significant effect of PEGylation on the dispersity enhancement, the dispersity of MGO and PMGO in different medium was further assessed. It appeared from Fig. 2C that MGO nanomaterials aggregated promptly in deionized water, normal saline, PBS, and DMEM medium, clearly indicating the necessity for enhancing the dispersity of MGO in physiological solutions for further application in biomimetic nanoengineering. On the contrary, it could be found that PMGO had a brilliant dispersity in deionized water and DMEM, which could keep stable at least 10 days. After 10 days, there was slight discoloration appeared in PBS and normal saline, which might be related to the mild aggregation of PMGO. Overall, surface PEGylation played a crucial part in improving the dispersity of MGO, which can be employed to settle the issue of PMGO aggregation in the top-down approach. The brilliant dispersity in PBS endowed PMGO with great interfacial interaction potential, which enabled it to be employed as a nanocarrier with high membrane coating rate.

In order to affirm whether PEGylation could improve the HM coating efficiency, we investigated the fluorescence property of HPMGO and HM coated MGO (HMGO) by fluorescence spectroscopy. As indicated in Fig. 2D, HPMGO and HMGO both exhibited a sharp emission peak appearing at around 525 nm originated from FITC, while the emission of HPMGO was found to be higher than that of HMGO. The difference indicated that due to the improved dispersity and increased contact area between GO

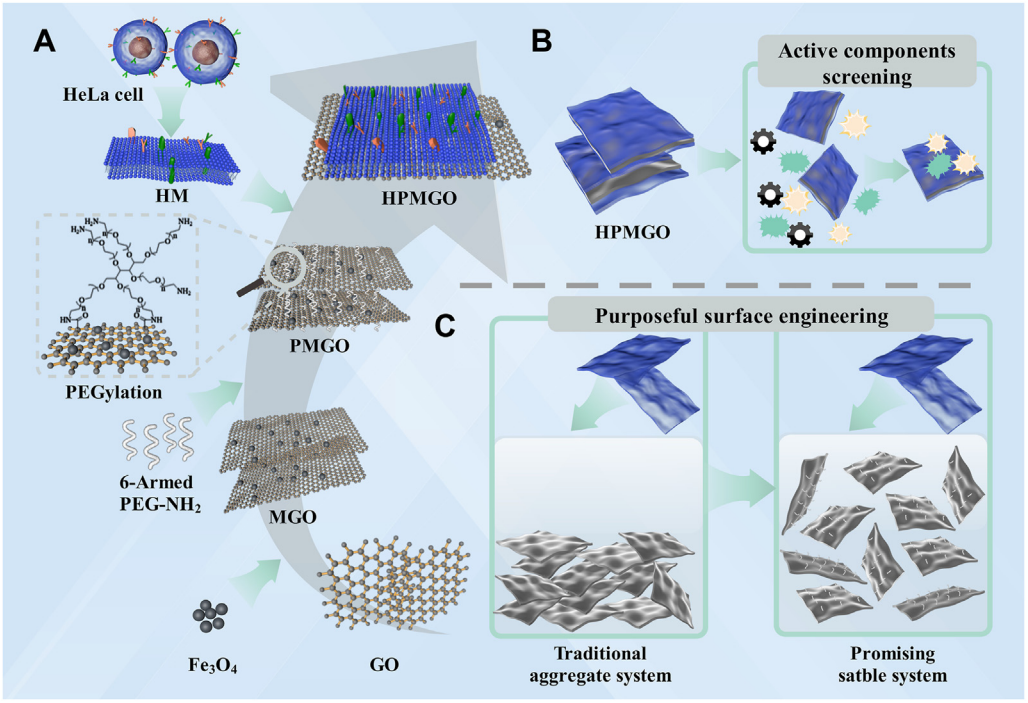

Figure 1 Schematic representation of (A) the preparation of HPMGO, (B) its application for drug leads capture, and (C) difference between traditional aggregation system and the promising PEGylated stable system.

and CM, PEGylated GO can increase the adsorption amount of HM on its surface.

3.3. *Characterization of HPMGO*

To confirm whether the PMGO has been fabricated as we expected, FTIR spectrums of GO and PMGO were first performed. As shown in Fig. 3A, both GO and PMGO exhibited a C−O stretching vibration peak (3411 cm^{-1}) and an −OH vibration peak (1634 cm^{-1}), which corresponded to the structure of GO. It is obvious that after PEGylation of MGO, the characteristic bands of C−H stretching vibration and C−O stretching vibration can be found at 2871 and 1102 cm^{-1}, respectively. Moreover, the bands at 587 cm^{-1} can be observed, which was assigned to the stretching vibration of Fe−O.

With a view to explore the element composition of PMGO before and after modification, XPS measurements were carried out. As presented in Fig. 3B, the presence of the N 1s peak in PMGO clearly demonstrated the attachment of PEG. From the thermal decomposition patterns of GO and PMGO displayed in TGA (Supporting Information Fig. S1), it can be seen that their weight losses were 60% and 40%, respectively, which revealed that the thermal stability of PMGO was enhanced after the attachment of PEG. This may be due to the crosslinking of PEG and GO, which enhanced the correlation between molecules, thus improving the thermal stability of PMGO.

Magnetization curves were obtained by VSM analysis. As can be seen from Fig. 3C, after PEGylation and HM coating, the saturation magnetization (Ms) of HPMGO was decreased. The decrease of Ms value could be ascribed to the existence of GO and HM, which reduced the content of Fe_3O_4 of the composites. However, there is still enough magnetism to allow rapid separation of HPMGO. As indicated in Fig. 3D, the zeta potential of PMGO is -0.73 ± 0.25 mV, which becomes more cationic after PEG modification, verifying the successful attach of positively charged amino groups to the PMGO surface. Subsequently, the zeta potential of HPMGO is -19.23 ± 0.74 mV, which close to that of the donor cells indicating that HM successful coating on the surface of PMGO, and presented in the right-side-out direction.

As depicted in Fig. 3E and Supporting Information Fig. S2, the structural morphologies of GO, PMGO, and HPMGO were studied by TEM and SEM. From TEM images of GO (Fig. 3E), it could be found that GO exhibited a sheet-liked structure with smooth surface. After attached with magnetic beads and PEG, PMGO were formed, and the size of the magnetic beads was around 200 nm. After being coated by HM, the transparency of HPMGO was lower than that of PMGO nanosheet, indicating that HM successfully coated PMGO. Furthermore, the SEM image of GO presented a sheet-like structure with small thickness and smooth surface as illustrated in Fig. S2. It can be seen that the nanolayer structure of PMGO still existed after magnetic modification and PEGylation, and the magnetic beads were successfully attached on the GO nanosheets. Subsequently, the surface of HPMGO is obviously rough, which was consistent with above structural morphologies results.

Furthermore, the optical properties of MGO and PMGO were examined by UV−Vis absorbance spectroscopy. As illustrated in Supporting Information Fig. S3, MGO and PMGO both revealed UV−Vis absorbance over a wide wavelength range, though the absorbance of PMGO was higher than that of MGO. The difference in absorbance could be attributed to the surface modification associated with the amidation of GO PEGylation, which was consistent with the previous report[33,34].

3.4. *Protein analysis and fluorescence characterization*

As the existence of specific receptors is the key to successfully target ligands. We confirmed the protein composition of HeLa

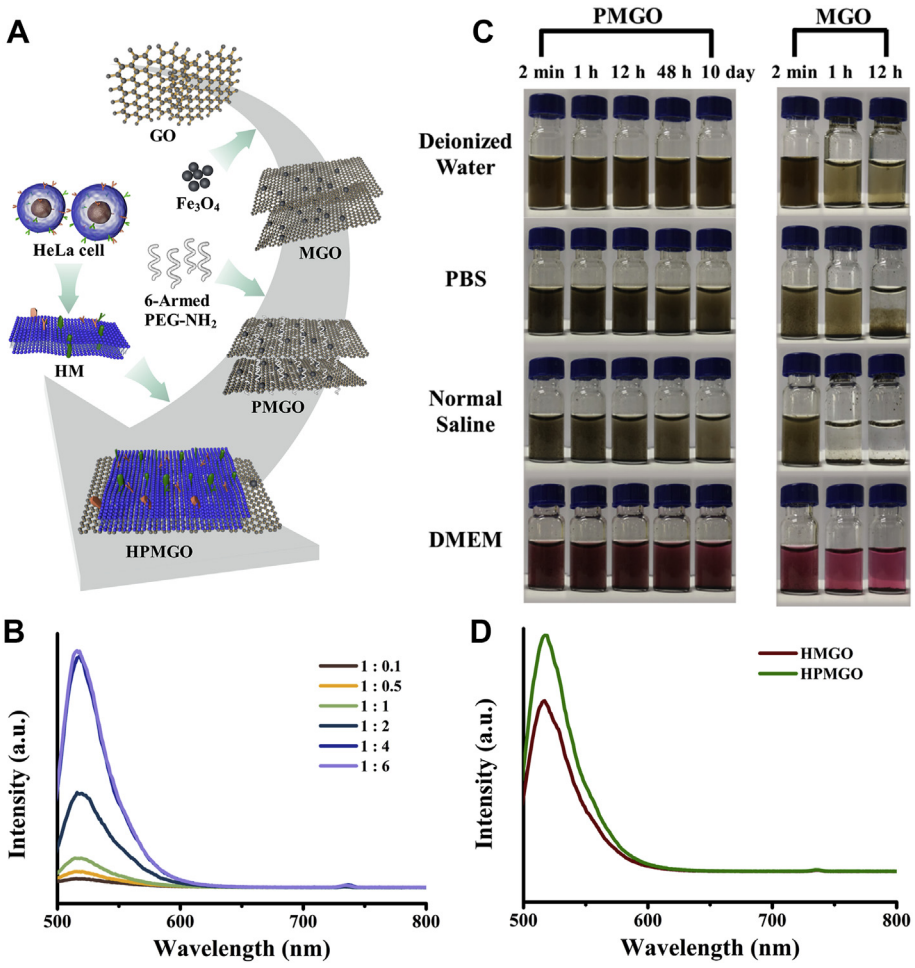

Figure 2 Preparation and dispersity evaluation of HPMGO. (A) Schematic illustration of synthesis of HPMGO. (B) Emission spectra of HPMGO prepared by HM/FITC and MGO at different ratios. (C) Digital photographs of MGO and PMGO in different medium. (D) Fluorescence property of HPMGO and HMGO.

cell, HM, and HPMGO by using SDS-PAGE. Protein analysis illustrated that membrane proteins of HeLa cells were well preserved during coating process as well as could be identified on HPMGO (Fig. 3F). To further study the HM coating, we conducted the CLSM to directly visualize the attachment of HM on the surface of PMGO. It can be seen from Fig. 3G that PMGO nanosheets could be wrapped by the membrane layer and endowed with a large number of ligand-targeting sites, which enabled HPMGO to have excellent targeting capability compared with bare PMGO.

3.5. *Adsorption capability of HPMGO*

Since the dispersity of PMGO was well improved, we then further investigated the adsorption capability of the prepared HPMGO. We used vinorelbine ditartrate as a model ligand to investigate the adsorption capability of HPMGO, and the binding amounts (Q) was used as an indicator to evaluate the capability. Various concentrations of vinorelbine ditartrate were incubated with HPMGO and PMGO, respectively, and the HPLC was employed to monitor the binding amounts. As illustrated in Fig. 4A, with the increase of concentration, the binding amounts of HPMGO to vinorelbine ditartrate increased rapidly at the initial stage, and then slowed down until reached saturation at 116.2 mg/g. Compared with PMGO (Q = 45.5 mg/g), the adsorption capability of HPMGO to vinorelbine ditartrate was significantly increased as the result that HM coating endowed it with a large number of specific receptors, providing active ligand targeting sites for vinorelbine ditartrate binding.

To better understand the adsorption process, Langmuir and Freundlich adsorption isotherm models were used to fit the adsorption data, and the equations as shown in Eqs. (3) and (4):

$$\frac{C_e}{Q_e} = \frac{1}{Q_{max}K_L} + \frac{1}{Q_{max}}C_e \tag{3}$$

$$\mathrm{Lg}Q_e = \mathrm{Lg}K_F + m\mathrm{Lg}C_e \tag{4}$$

where Q_{max} (mg/g) refers to the maximum adsorption capacity. K_L (L/g) refers to adsorption constants of Langmuir and K_F (mg/g) refers to adsorption constants of Freundlich. And n is heterogeneity factor. The adsorption isotherms data were fitted by Langmuir and Freundlich models (Supporting Information Fig. S4) to obtain relevant parameters (Supporting Information Table S1). According to the values of correlation coefficient (r), the

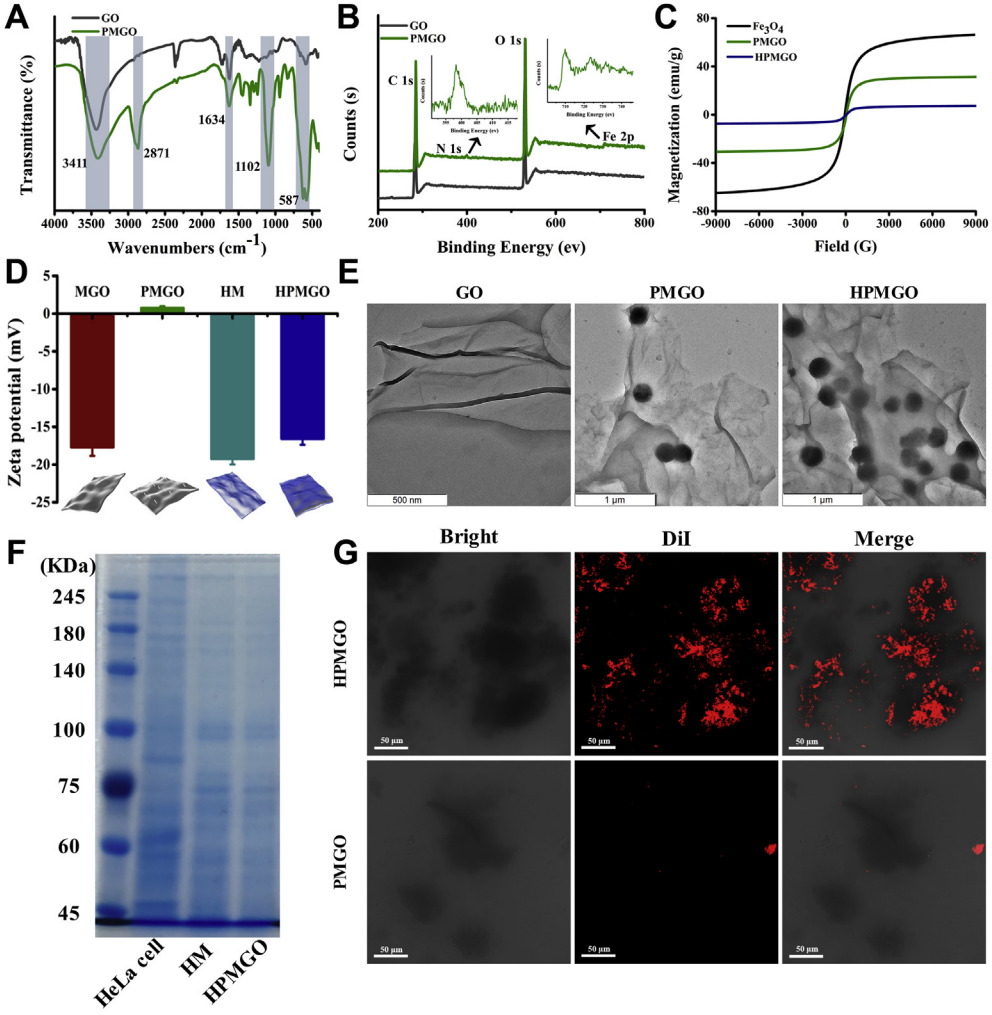

Figure 3 Characterization of HPMGO. (A) FTIR spectra of GO and PMGO. (B) XPS patterns of GO and PMGO. (C) Magnetic hysteresis loops of Fe_3O_4, PMGO, and HPMGO. (D) Zeta potential results of MGO, PMGO, HM, and HPMGO. (E) TEM images of GO (scale bar = 500 nm), PMGO (scale bar = 1 μm), and HPMGO. (scale bar = 1 μm). (F) Membrane protein analysis of HeLa cells, HM, and HPMGO. (G) Confocal microscopy images of HPMGO and PMGO labelled with DiI (red). Scale bar = 50 μm.

adsorption behavior was more consistent with the Langmuir model, indicating a monolayer sorption of vinorelbine ditartrate on the surface of HPMGO.

3.6. *Adsorption kinetics of HPMGO*

The adsorption kinetics of HPMGO and PMGO for vinorelbine ditartrate adsorption were presented in Fig. 4B. Accordingly, the adsorption rate of HPMGO to vinorelbine ditartrate was fast. Because of the abundant adsorption sites, it can achieve half of its saturation adsorption within 3 min. After only 6 min, the adsorption reached equilibrium. Compared with HPMGO, PMGO had a slow adsorption rate and small adsorption amount. High adsorption efficiency of HPMGO might be due to the abundant target sites on its surface.

In this study, the pseudo-first-order (PFO) and pseudo-second-order (PSO) equations were applied to fit the adsorption kinetic data. The equations as shown in Eqs. (5) and (6):

$$\mathrm{Log}(q_e - q_t) = \mathrm{Log}q_e - \frac{k_1 t}{2.303} \tag{5}$$

$$\frac{t}{q_t} = \frac{1}{k_2 q_e^2} + \frac{t}{q_0} \tag{6}$$

where q_e (mg/g) and q_t (mg/g) refer to the equilibrium adsorption capacity and the adsorption capacity at a certain time (min), respectively. k_1 (min^{-1}) represents the adsorption rate constants of PFO model, and k_2 (g/mg/min) represents the adsorption rate constants of PSO model. Both HPMGO and PMGO presented a better correlation with the PSO model (Supporting Information Table S2), indicating that the adsorption was related to the number of binding sites.

3.7. *Adsorption selectivity of HPMGO*

Furthermore, to verify the selectivity of HPMGO in capture specific ligands, we challenged our detection by using other drugs acting on different receptors. In this study, vinorelbine ditartrate was used as the target drug, while verapamil, tamsulosin, and valsartan were applied as the negative controls. As depicted in Fig. 4C, compared to the negative controls, the

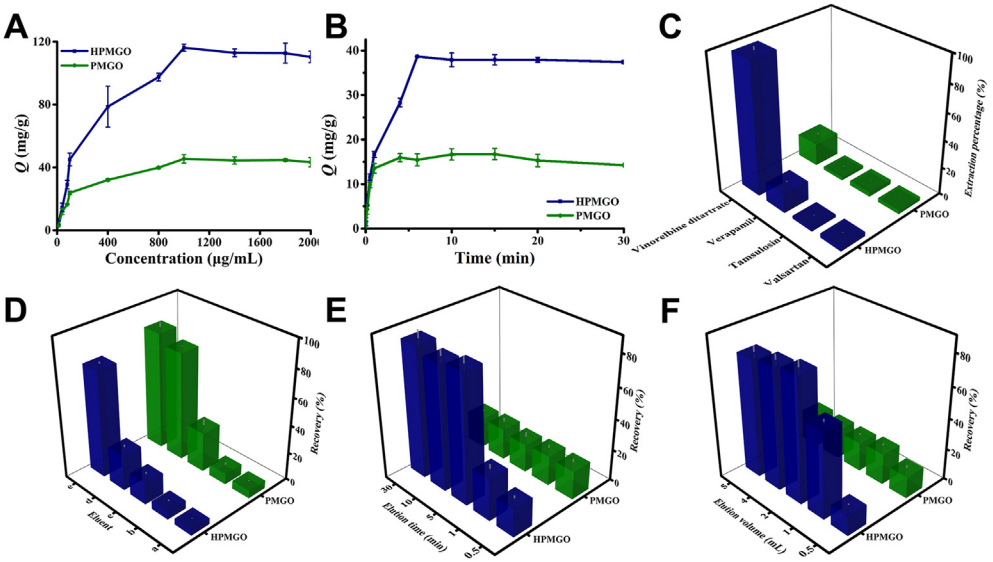

Figure 4 (A) Static adsorption isotherm curves. (B) Dynamic adsorption curves. (C) Adsorption selectivity results. (D) Selection of washing and elution solution: (a) water, (b) PBS, (c) 10% methanol solution, (d) PBS-acetonitrile (9:1, *v*/*v*), and (e) PBS-acetonitrile (7:3, *v*/*v*). (E) Optimization of elution time. (F) Optimization of elution volume.

adsorption capacity of positive drug vinorelbine ditartrate by HPMGO was higher, which demonstrated stronger binding capacity of vinorelbine ditartrate to HPMGO, supporting the existence of ligand targeting sites. Clearly, all the encouraging results indicated that the HM coating could firmly endow HPMGO with rich ligand targeting sites and enhance its adsorption performance for specific ligands. Therefore, sensitive and selective detection of the proposed drug leads capture platform is feasible.

3.8. *Screening conditions optimization*

Based on the well-preserved membrane activity and target adsorption capability of HPMGO, we then envision the potential application of HPMGO in efficient screening of active components, where HPMGO was employed as the adsorbent. Hence, several experimental parameters were optimized for efficient ligands capture. Firstly, in order to obtain a high recovery, the washing solvent and elution solvent were optimized. Specifically, five solvents [water (a), PBS (b), 10% methanol solution (c), PBS-acetonitrile (9:1, *v*/*v*; d), and PBS-acetonitrile (7:3, *v*/*v*; e)] were investigated. As shown in Fig. 4D, we can see that the maximum recovery was obtained when employed the PBS-acetonitrile (7:3, *v*/*v*) as elution solvent, while PBS-acetonitrile (9:1, *v*/*v*) had better elution ability for PMGO, but had no obvious influence on HPMGO. Therefore, 9:1 and 7:3 PBS-acetonitrile were applied as the washing solvent and elution solvent, respectively. Besides, elution time and eluent volume, which might influence the recovery of adsorbate, were also optimized. As the results depicted in Fig. 4E, the recovery positively correlated with the elution time from 0.5 to 30 min and reached stable after 5 min, indicating that the elution procedure can be essentially completed in 5 min. In addition, since the recovery can reach the maximum when the solution volume was larger than 2 mL, 2 mL was taken as the elution volume.

3.9. *Potential active components screening from TCM*

To evaluate the batch to batch variation of the HPMGO nanodecoys, the adsorption capacity of six batches of HPMGO was studied. The average adsorption capacity of the six batches of HPMGO was 45.33 mg/g, and the relative standard deviation (RSD) was 6.8%, indicating that HPMMGO had good reproducibility.

Despite many efforts and advances have been made in the screening of active components in TCM in recent decades, the screening of potential active components from TCM is still an expensive, complex, time-consuming, and laborious process without a guarantee of success. In this context, biomimetic affinity recognition technology has become a promising strategy with the advantage of directly simulating drug interactions *in vivo*, detecting the affinity of different ligands to membrane receptors, and screening potential active components. In consideration of the critical role of PEGylation in improving dispersity of MGO, this work introduced PEGylation to solve the problem of easy aggregation of nanocarriers in the top-down approach to improve the affinity recognition efficiency.

A. dahurica is a TCM that has been used in the therapy for pain, furunculosis, abscesses, and acne. In previous studies, *A. dahurica* exhibited diverse biological activities, including antitumor[38], antiinflammatory[39], antioxidant[40], and anti-allergic effects[41]. Inspired by these biological activities, we hypothesize that *A. dahurica* cotains compounds that could bind to HeLa cells. Therefore, taking *A. dahurica* as an example, the screening of potential active components from TCM was carried out to validate the practical application of the designed HPMGO. The schematic was illustrated in Fig. 5A. As a result, there were three intensive peaks can be observed in the elution (Fig. 5B), which may be the potential active compounds screened by HPMGO. The adsorption of these compounds on HPMGO indicated that they were ligands of the HM receptor since binding between them. Furthermore, the

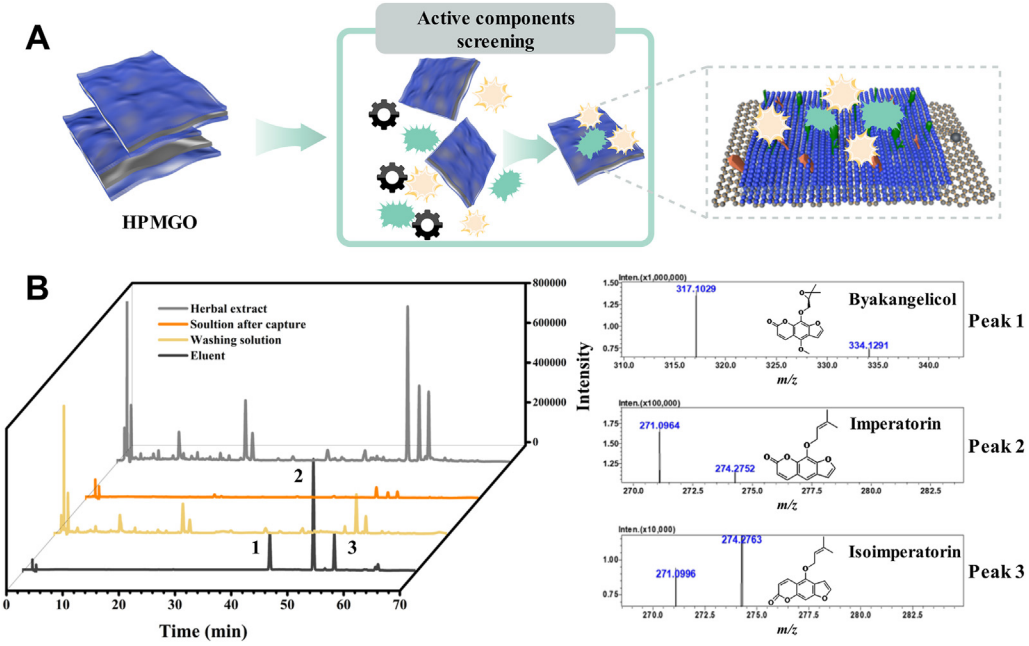

Figure 5 (A) Schematic illustration of drug leads capture from complex herbal matrices. (B) Chromatograms of the practical application using HPMGO and TOFMS results of peaks 1, 2 and 3.

screened active components were identified as byakangelicol, imperatorin, and isoimperatorin, respectively, using HPLC−Q-TOF-MS/MS, and verified by corresponding standards. The above three components are coumarins in *Angelica dahuricae*. Although the coumarins in *A. dahuricae* are similar in structure, other coumarins have not been screened out, possibly due to their different contents and pharmacological activity. The above results indicated that the CM affinity recognition platform can selectively screen potential active components from TCM with high reliability.

3.10. *In vitro antiproliferative activity*

The evaluation of the antiproliferative efficacy of the screened active components was subsequently performed *in vitro* by CCK-8 assay. After treated with byakangelicol, imperatorin, and isoimperatorin at different concentrations (0.78, 1.56, 3.125, 6.25, 25 and 100 μg/mL), cell viability of HeLa cells was determined by microplate reader. As expected, cell viability all decreased with increasing concentration, which clearly demonstrated the efficiency of prepared drug leads capture platform by the receptor−ligand interaction (Fig. 6A). The half-maximal inhibitory concentrations (IC_{50}) of byakangelicol and isoimperatorin were 22.65 ± 1.21 and 11.89 ± 1.24 μg/mL, respectively. However, the inhibition of imperatorin on HeLa cells did not reach 50% in the range of 0.78−100 μg/mL, revealing that the antiproliferative efficacy of imperatorin was weaker than that of the other two compounds. In addition, according to the contents of byakangelicol, imperatorin, and isoimperatorin in *A. dahuricae* extract, we mixed these compounds at the similar concentration to get the artificial mixture. And then compared the cytotoxicity of HeLa cells incubated with the artificial mixture and *A. dahurica*. As depicted in Supporting Information Fig. S5, the cytotoxicity of *A. dahurica* extract was slightly higher than that of the mixture, which may be due to the presence of a small amount of other active components in the *A. dahurica* extract.

3.11. *Cell apoptosis analysis*

As byakangelicol, imperatorin, and isoimperatorin showed potent antiproliferative activity on HeLa cells, hoechst 33,258 staining assay was further carried out to investigate its ability to induce apoptosis of HeLa cells. As illustrated in Fig. 6B, after treatment of HeLa cells with byakangelicol, imperatorin, and isoimperatorin for 48 h, respectively, the typical apoptotic characteristics including decreased cell number, cell contraction, and nuclear condensation were appeared, which suggested that all the compounds could induce apoptosis of HeLa cells.

To further confirm the effect of above three active compounds on induction of apoptosis in HeLa cells, an annexin FITC/PI staining assay was also conducted. HeLa cells were treated with byakangelicol, imperatorin, and isoimperatorin at different concentrations, and the flow cytometry analysis results were depicted in Fig. 6C. The result showed that byakangelicol, imperatorin, and isoimperatorin could induce apoptosis in a concentration-dependent manner. The apoptosis rates of HeLa cells induced by byakangelicol were 10.3%, 26.0%, and 36.9% at 10, 20, and 40 μg/mL, respectively. The apoptosis rates of HeLa cells induced by imperatorin were 11.4%, 15.3%, and 39.7% at 10, 20, and 40 μg/mL, respectively. The apoptosis rates of HeLa cells induced by isoimperatorin were 10.4%, 17.7%, and 62.8% at 10, 20, and 40 μg/mL, respectively. In addition, a positive control, vinorelbine ditartrate, induced 10.8%, 25.9%, and 83.6% apoptosis in HeLa cells at 0.01, 0.05, and 0.1 μg/mL, respectively. Moreover, we also compared the apoptosis of HeLa cells incubated with the artificial mixture and *A. dahurica*. As shown in Supporting Information Fig. S6, the apoptosis rates induced by the artificial mixture and *A. dahurica* were 36.6% and 44.5%, respectively.

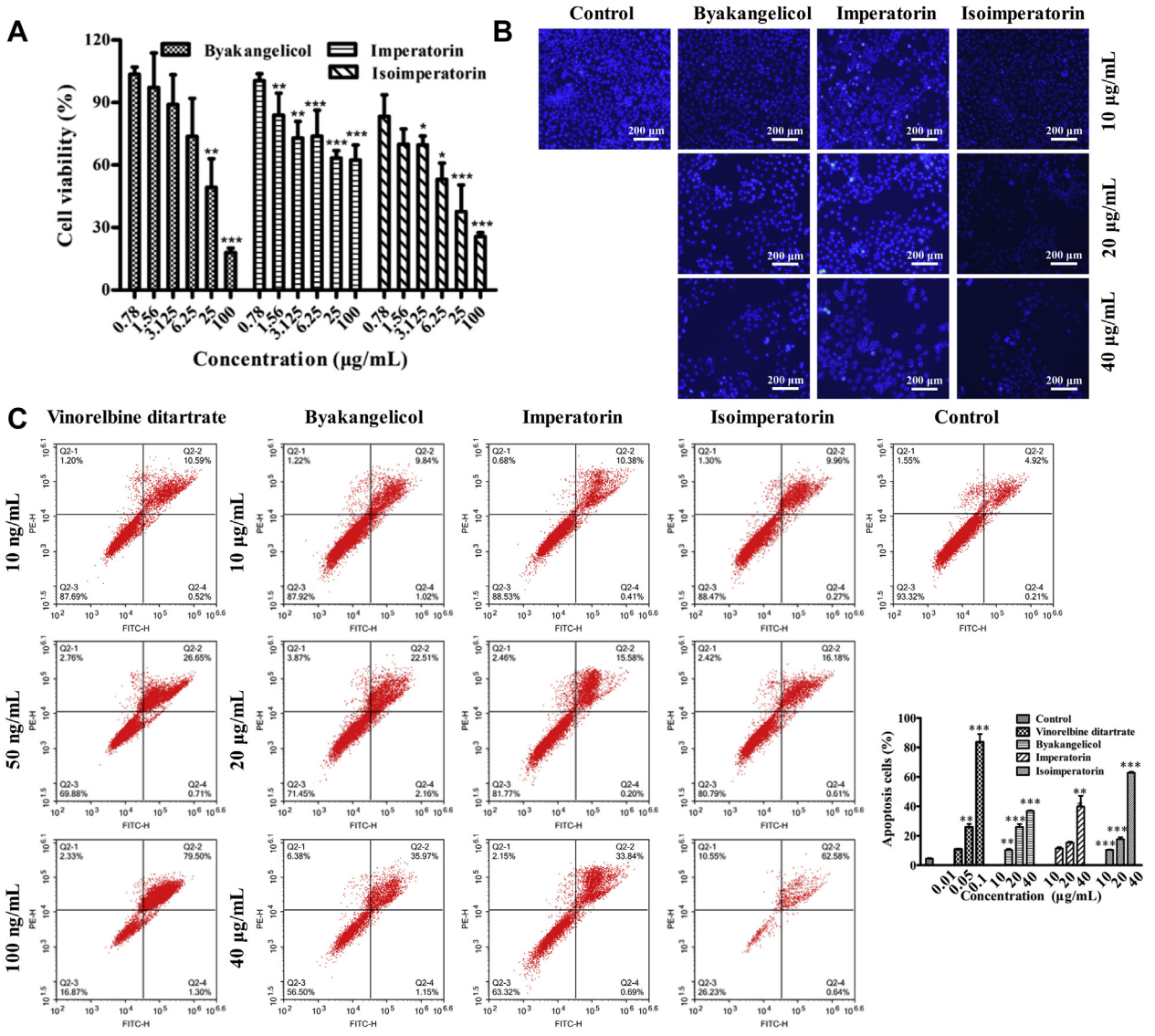

Figure 6 (A) Effect of byakangelicol, imperatorin, and isoimperatorin on the cell growth of HeLa cells. (B) Hoechst 33,258 staining of byakangelicol, imperatorin, and isoimperatorin on HeLa cells and DMSO treatment group was used as control. Scale bar = 200 μm. (C) Apoptotic effects of byakangelicol, imperatorin, and isoimperatorin on HeLa cells. Cells were incubated with the different concentrations for 48 h and detected using Annexin V-FITC/PI staining by flow cytometry. Data are presented as mean ± SD ($n = 3$). *$P < 0.05$, **$P < 0.01$, and ***$P < 0.001$ *vs.* control group.

4. Conclusions

Summarily, based on purposeful surface engineering, a novel CM biomimetic graphene nanodecoy was developed for active components screening from TCM with enhanced efficiency. Specifically, PMGO was fabricated by covalently grafting 6-armed PEG−NH_2 onto the surface of MGO, and was used as a high dispersity HM coating nanocarrier for preparing nanodecoy with enhanced coating efficiency and screening ability. The nanostructure and dispersity of prepared PMGO and HPMGO were well characterized. The constructed PMGO possessed enhanced physiological stability and biocompatibility, which could keep stable at least 10 days, and the CM coating efficiency was further improved. Notably, the prepared HPMGO can be used as nanodecoys for screening of active components from TCM. *In vitro* antiproliferative activity and cell apoptosis analysis demonstrated that the screened compounds by HPMGO could induced HeLa cells apoptosis in a concentration-dependent manner, indicating an aussichtsreich prospect in the ligand targeting field. Significantly, this accurately controlled coating strategy holds great promise for the customization applications of CM-camouflage nanomaterials, which would further promote the design of more effective nanoplatforms for active components screening from TCM.

Acknowledgments

We gratefully acknowledge the National Natural Science Foundation of China (Nos. 82073807 and 81973277), and the World-Class Universities (Disciplines) and the Characteristic Development Guidance Funds for the Central Universities (No. PY3A012, China) for financial support. We thank Dr. Hao at the Instrument

Analysis Center of Xi'an Jiaotong University for their assistance with CLSM analysis.

Author contributions

Qi Hu designed and performed the experiments, interpreted the data, and wrote the manuscript. Lanlan Jia, Xiaolin Zhang, and Aihong Zhu participated part of the experiments. Sicen Wang revised the manuscript. Xiaoyu Xie conceived the study and revised the manuscript. All of the authors have read and approved the final manuscript.

Conflicts of interest

The authors have no conflicts of interest to declare.

Appendix A. Supporting information

Supporting data to this article can be found online at https://doi.org/10.1016/j.apsb.2021.05.021.

References

1. Hu CMJ, Fang RH, Wang KC, Luk BT, Thamphiwatana S, Dehaini D, et al. Nanoparticle biointerfacing by platelet membrane cloaking. *Nature* 2015;**526**:118−21.
2. Li JC, Zhen X, Lyu Y, Jiang YY, Huang JG, Pu KY. Cell Membrane coated semiconducting polymer nanoparticles for enhanced multimodal cancer phototheranostics. *ACS Nano* 2018;**12**:8520−30.
3. Xuan MJ, Shao JX, Li JB. Cell membrane-covered nanoparticles as biomaterials. *Natl Sci Rev* 2019;**6**:551−61.
4. Li RX, He YW, Zhang SY, Qin J, Wang JX. Cell membrane-based nanoparticles: a new biomimetic platform for tumor diagnosis and treatment. *Acta Pharm Sin B* 2018;**8**:14−22.
5. Gong H, Chen F, Huang ZL, Gu Y, Zhang QZ, Chen YJ, et al. Biomembrane-modified field effect transistors for sensitive and quantitative detection of biological toxins and pathogens. *ACS Nano* 2019;**13**:3714−22.
6. Chang ZM, Zhang R, Yang C, Shao D, Tang YG, Dong WF, et al. Cancer-leukocyte hybrid membrane-cloaked magnetic beads for the ultrasensitive isolation, purification, and non-destructive release of circulating tumor cells. *Nanoscale* 2020;**12**:19121−8.
7. Zhang Y, Chen YJ, Lo C, Zhuang J, Angsantikul P, Zhang QZ, et al. Inhibition of pathogen adhesion by bacterial outer membrane-coated nanoparticles. *Angew Chem Int Ed* 2019;**58**:11404−8.
8. Kuerban K, Gao XW, Zhang H, Liu JY, Dong MX, Wu LN, et al. Doxorubicin-loaded bacterial outer-membrane vesicles exert enhanced anti-tumor efficacy in non-small-cell lung cancer. *Acta Pharm Sin B* 2020;**10**:1534−48.
9. Kroll AV, Fang RH, Jiang Y, Zhou JR, Wei XL, Yu CL, et al. Nanoparticulate delivery of cancer cell membrane elicits multiantigenic antitumor immunity. *Adv Mater* 2017;**29**:1703969.
10. Zhen X, Cheng PH, Pu KY. Recent advances in cell membrane-camouflaged nanoparticles for cancer phototherapy. *Small* 2019;**15**:1804105.
11. Wei XL, Zhang G, Ran D, Krishnan N, Fang RH, Gao WW, et al. T-cell-mimicking nanoparticles can neutralize HIV infectivity. *Adv Mater* 2018;**30**:1802233.
12. Wei XL, Ran D, Campeau A, Xiao C, Zhou JR, Dehaini D, et al. Multiantigenic nanotoxoids for antivirulence vaccination against antibiotic-resistant gram-negative bacteria. *Nano Lett* 2019;**19**:4760−9.
13. Chen YJ, Zhang Y, Chen MC, Zhuang J, Fang RH, Gao WW, et al. Biomimetic nanosponges suppress *in vivo* lethality induced by the whole secreted proteins of pathogenic bacteria. *Small* 2019;**15**:1804994.
14. Chen XF, Wu YL, Chen C, Gu YQ, Zhu CY, Wang SP, et al. Identifying potential anti-COVID-19 pharmacological components of traditional Chinese medicine Lianhuaqingwen capsule based on human exposure and ACE2 biochromatography screening. *Acta Pharm Sin B* 2021;**11**:222−36.
15. Hu Q, Bu YS, Cao RQ, Zhang G, Xie XY, Wang SC. Stability designs of cell membrane cloaked magnetic carbon nanotubes for improved life span in screening drug leads. *Anal Chem* 2019;**91**:13062−70.
16. Sherwood J, Sowell J, Beyer N, Irvin J, Stephen C, Antone AJ, et al. Cell-membrane coated iron oxide nanoparticles for isolation and specific identification of drug leads from complex matrices. *Nanoscale* 2019;**11**:6352−9.
17. Hu CMJ, Fang RH, Luk BT, Chen KNH, Carpenter C, Gao WW, et al. 'Marker-of-self' functionalization of nanoscale particles through a top-down cellular membrane coating approach. *Nanoscale* 2013;**5**:2664−8.
18. Hu CMJ, Zhang L, Aryal S, Cheung C, Fang RH, Zhang LF. Erythrocyte membrane-camouflaged polymeric nanoparticles as a biomimetic delivery platform. *Proc Natl Acad Sci U S A* 2011;**108**:10980−5.
19. Auffan M, Rose J, Bottero JY, Lowry GV, Jolivet JP, Wiesner MR. Towards a definition of inorganic nanoparticles from an environmental, health and safety perspective. *Nat Nanotechnol* 2009;**4**:634−41.
20. Patel P, Santo KP, Burgess S, Vishnyakov A, Neimark AV. Stability of lipid coatings on nanoparticle-decorated surfaces. *ACS Nano* 2020;**14**:17273−84.
21. Zhu JY, Zhang MK, Zheng DW, Yang B, Ma N, Li RQ, et al. A biohybrid lurker-to-attacker strategy to solve inherent dilemma of positively charged delivery nanoparticles. *Chem Mater* 2017;**29**:2227−31.
22. Zhu JY, Zhang MK, Zheng DW, Hong S, Feng J, Zhang XZ. A universal approach to render nanomedicine with biological identity derived from cell membranes. *Biomacromolecules* 2018;**19**:2043−52.
23. Geim AK. Graphene: status and prospects. *Science* 2009;**324**:1530−4.
24. Kim H, Lee D, Kim J, Kim TI, Kim WJ. Photothermally triggered cytosolic drug delivery *via* endosome disruption using a functionalized reduced graphene oxide. *ACS Nano* 2013;**7**:6735−46.
25. Sung SY, Su YL, Cheng W, Hu PF, Chiang CS, Chen WT, et al. Graphene quantum dots-mediated theranostic penetrative delivery of drug and photolytics in deep tumors by targeted biomimetic nanosponges. *Nano Lett* 2019;**19**:69−81.
26. Du WC, Wu HG, Chen HW, Xu GC, Li C. Graphene oxide in aqueous and nonaqueous media: dispersion behaviour and solution chemistry. *Carbon* 2020;**158**:568−79.
27. Hu Q, Zhang XL, Jia LL, Zhen XY, Pan XY, Xie XY, et al. Engineering biomimetic graphene nanodecoys camouflaged with the EGFR/HEK293 cell membrane for targeted capture of drug leads. *Biomater Sci* 2020;**8**:5690−7.
28. Patil R, Bahadur P, Tiwari S. Dispersed graphene materials of biomedical interest and their toxicological consequences. *Adv Colloid Interfac* 2020;**275**:102051.
29. Nandanapalli KR, Mudusu D, Lee S. Functionalization of graphene layers and advancements in device applications. *Carbon* 2019;**152**:954−85.
30. Zalipsky S. Chemistry of polyethylene-glycol conjugates with biologically-active molecules. *Adv Drug Deliv Rev* 1995;**16**:157−82.
31. Li J, Kao WJ. Synthesis of polyethylene glycol (PEG) derivatives and PEGylated-peptide blopolymer conjugates. *Biomacromolecules* 2003;**4**:1055−67.
32. Liu Z, Robinson JT, Sun XM, Dai HJ. PEGylated nanographene oxide for delivery of water-insoluble cancer drugs. *J Am Chem Soc* 2008;**130**:10876−7.
33. Kim H, Kim WJ. Photothermally controlled gene delivery by reduced graphene oxide-polyethylenimine nanocomposite. *Small* 2014;**10**:117−26.

34. Ma G, Qi JJ, Cui QF, Bao XY, Gao D, Xing CF. Graphene oxide composite for selective recognition, capturing, photothermal killing of bacteria over mammalian cells. *Polymers* 2020;**12**:1116.
35. Xu ZY, Wang S, Li YJ, Wang MW, Shi P, Huang XY. Covalent functionalization of graphene oxide with biocompatible poly(ethylene glycol) for delivery of paclitaxel. *ACS Appl Mater Interfaces* 2014;**6**:17268−76.
36. Ding X, Cao Y, Yuan YF, Gong ZR, Liu Y, Zhao L, et al. Development of APTES-decorated HepG2 cancer stem cell membrane chromatography for screening active components from *Salvia miltiorrhiza*. *Anal Chem* 2016;**88**:12081−9.
37. Li D, Muller MB, Gilje S, Kaner RB, Wallace GG. Processable aqueous dispersions of graphene nanosheets. *Nat Nanotechnol* 2008;**3**:101−5.
38. Lee SH, Han AR, Kang U, Kim JB, Seo EK, Jung CH. Inhibitory effects of furanocoumarins from the roots of *Angelica dahurica* on ionizing radiation-induced migration of A549 human non-small cell lung cancer cells. *Nat Prod Commun* 2020;**15**:1−6.
39. Yang WQ, Song YL, Zhu ZX, Su C, Zhang X, Wang J, et al. Anti-inflammatory dimeric furanocoumarins from the roots of *Angelica dahurica*. *Fitoterapia* 2015;**105**:187−93.
40. Zheng YM, Shen JZ, Wang Y, Lu AX, Ho WS. Anti-oxidant and anti-cancer activities of *Angelica dahurica* extract *via* induction of apoptosis in colon cancer cells. *Phytomedicine* 2016;**23**:1267−74.
41. Li D, Wu L. Coumarins from the roots of *Angelica dahurica* cause anti-allergic inflammation. *Exp Ther Med* 2017;**14**:874−80.